Precision estimation of time delay based on weak measurement with real weak value

Weining Liu [ORCID],[1] Yisen Wang [ORCID],[1,*] and Hailu Luo[2]

[1]*GBA Branch of Aerospace Information Research Institute, Chinese Academy of Sciences,
and Guangdong Provincial Key Laboratory of Terahertz Quantum Electromagnetics, Guangzhou 510700, China*
[2]*Laboratory for Spin Photonics, School of Physics and Electronics, Hunan University, Changsha 410082, China*

In the standard weak measurement, the imaginary part of the weak value is usually constructed with a specific pre- or postselection state to cause a large shift of the frequency-domain pointer. In this paper we demonstrate that the purely real weak value can also shift the frequency-domain pointer when using a broad-spectrum light source. The reason for the deflection of the frequency-domain pointer in this scheme is that the postselection probability of different frequency is different, which causes the rearrangement of the amplitudes of the spectrum. The weak measurement with real weak value can be used for the estimation of time delay, and it is found that it can reach the same high resolution as the standard weak measurement in some sensitive regions.

I. INTRODUCTION

The concept of weak measurement was first proposed by Aharonov *et al.* [1], and has been widely discussed due to its advantages in small parameter measurement [2–5]. Weak measurement is a high-precision measurement scheme different from the standard interferometry scheme. In weak measurement, the amplified physical signals can be obtained in the pointer through appropriate preselection and postselection of the system to be measured. At the same time, unlike traditional eigenvalues, a weak value can be taken outside the range of eigenvalue, or even a complex number [6].

In the frequency-domain weak measurement, the ultrasmall time delay can be characterized by the output spectral distribution [7,8]. The change of time delay will affect the output spectrum, and this effect is drastic in some regions, which greatly improves the measurement precision of time delay [9,10]. The frequency-domain weak measurement can be employed in many applications, such as liquid concentration detection [11], optical rotation detection [12,13], ultra-small-pressure detection [14], and magneto-optical Kerr effect detection [15].

Reference [16] demonstrated that the imaginary weak value combined with the frequency-domain pointer can significantly improve the measurement precision of time delay, while the scheme with real weak value is less accurate than standard interferometry, although it can amplify the shift of the time-domain pointer. Therefore people focus on the application of an imaginary weak value in parameter estimation [17–19]. In the scheme with imaginary weak value, the step of preselection or postselection usually requires the combination of polarizer and quarter-wave plate (QWP). However, we must consider the effect of the wavelength dependence of the QWP when using a broad-spectrum light source [20]. Recently, Ref. [21] took an optical frequency comb as an

example to demonstrate that the result of frequency-domain weak measurement is a rearrangement of the spectrum amplitudes, which does not actually cause a shift of the comb teeth. The change of the probability distribution of frequency is due to the destructive interference of the system during postselection. Although it has been proved that the real weak value combined with time-domain analysis cannot improve the measurement precision, we found that the scheme with real weak value using a broad-spectrum light source can have an effect on the output spectrum due to destructive interference. The real weak value can also affect the frequency-domain pointer similarly to the imaginary weak value and can be used for high-precision parameter measurement.

In this paper, the weak measurement with real weak value (Re-WV) scheme is analyzed and discussed in the frequency domain, and the results are compared with the weak measurement with imaginary weak value (Im-WV) scheme. We compare the wavelength shift and measurement precision of the Re-WV scheme and the Im-WV scheme in different sensitive regions. We analyze the reason for the wavelength shift and the variation of spectrum in the Re-WV scheme. To demonstrate the potential of the Re-WV scheme for high-precision measurement, we discuss the Fisher information and the precision limit in this scheme.

II. THE WEAK MEASUREMENT WITH IMAGINARY WEAK VALUE

The weak measurement scheme usually includes three steps: firstly, the preselection state $|\psi_i\rangle$ is prepared for the system to be measured, then the pointer $|\varphi\rangle$ is weakly coupled with the system, and finally the joint state is postselected to the state $|\psi_f\rangle$ that is nearly orthogonal to the state $|\psi_i\rangle$ before measuring on the pointer. The weak value is defined as

$$A_w = \frac{\langle\psi_f|\hat{A}|\psi_i\rangle}{\langle\psi_f|\psi_i\rangle},\tag{1}$$
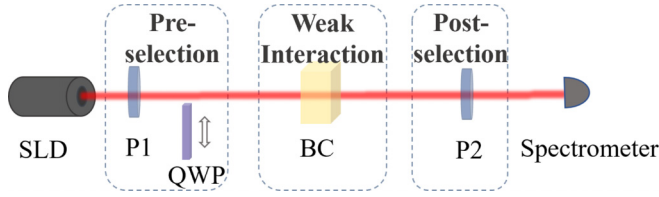
---

*wangyisen@aircas.ac.cn

FIG. 1. Diagram of the experimental setup of the weak measurement. P1, P2: polarizer; QWP: quarter-wave plate; BC: birefringent crystal. The broad-spectrum white light source is incident into the spectrometer after preselection, weak interaction, and postselection. The preselection process of the Im-WV scheme is completed by P1 and QWP, and the preselection process of the Re-WV scheme is completed by P1.

where $\hat{A}$ is the observable operator of the system. The experimental setup for measuring time delay is shown in Fig. 1. In this scheme we need to measure the small time delay introduced by a birefringent crystal between the horizontal and vertical polarization components, so the observable operator of the system is $\hat{A} = |H\rangle\langle H| - |V\rangle\langle V|$. The polarization degree of freedom of the input beam is used as the system to be measured, and the spectral distribution of the broad-spectrum light source is used as the pointer.

Here, we consider that the preselection state $|\psi_i\rangle$ is prepared by a polarizer P1 set to $\pi/4 + \varepsilon$ and a zero-order QWP set to $\pi/4$. The light beam is postselected at an angle of $-\pi/4$ by polarizer P2, which is nearly orthogonal to P1. Since the phase difference produced by the QWP is wavelength dependent, when the broad-spectrum linearly polarized light passes through the QWP, the Jones matrix can be written as

$$
\begin{bmatrix}
\cos\frac{\pi\lambda_0}{4\lambda} & -i\sin\frac{\pi\lambda_0}{4\lambda} \\
-i\sin\frac{\pi\lambda_0}{4\lambda} & \cos\frac{\pi\lambda_0}{4\lambda}
\end{bmatrix},
\tag{2}
$$

where λ_0 is the central wavelength of the input light. So the preselection state and the postselection state can be written as

$$
|\psi_i\rangle = \frac{1}{\sqrt{2}}\Big[\big(\cos\varepsilon - e^{i\frac{\pi\lambda_0}{2\lambda}}\sin\varepsilon\big)|H\rangle
$$

$$
+ \big(\cos\varepsilon + e^{i\frac{\pi\lambda_0}{2\lambda}}\sin\varepsilon\big)|V\rangle\Big],
\tag{3}
$$

$$
|\psi_f\rangle = \frac{1}{\sqrt{2}}(|H\rangle - |V\rangle),
\tag{4}
$$

where ε is defined as the preselection angle that can be adjusted. From Eq. (1) combined with $\omega = 2\pi c/\lambda$, the weak value can be obtained as

$$
A_w = -\cos\left(\frac{\pi\omega}{2\omega_0}\right)\cot\varepsilon + i\sin\left(\frac{\pi\omega}{2\omega_0}\right)\cot\varepsilon.
\tag{5}
$$

Considering the wavelength dependence of the preselection state, the weak value is complex instead of purely imaginary [20]. Assuming that the spectral distribution of the broad-spectrum light source is Gaussian, then the pointer state can be expressed as $|\varphi\rangle = \int d\omega f(\omega)|\omega\rangle$, where $f(\omega) = \frac{1}{\sqrt[4]{\pi\sigma^2}}\exp(-\frac{(\omega-\omega_0)^2}{4\sigma^2})$ is the wave function of the spectral distribution, and σ corresponds to the width of the spectrum. The

joint state after preselection can be expressed as

$$
|\Phi_i\rangle = \int d\omega \frac{f(\omega)}{\sqrt{2}}\Big[\big(\cos\varepsilon - e^{i\frac{\pi\omega}{2\omega_0}}\sin\varepsilon\big)|H\rangle
$$

$$
+ \big(\cos\varepsilon + e^{i\frac{\pi\omega}{2\omega_0}}\sin\varepsilon\big)\Big]|V\rangle|\omega\rangle.
\tag{6}
$$

After the weak interaction, there is a small time delay 2τ between the horizontal and vertical polarization components, so the joint state after the weak interaction can be expressed as

$$
|\Phi_i'\rangle = \int d\omega \frac{f(\omega)}{\sqrt{2}}\Big[e^{i\omega\tau}\big(\cos\varepsilon - e^{i\frac{\pi\omega}{2\omega_0}}\sin\varepsilon\big)|H\rangle
$$

$$
+ e^{-i\omega\tau}\big(\cos\varepsilon + e^{i\frac{\pi\omega}{2\omega_0}}\sin\varepsilon\big)|V\rangle\Big]|\omega\rangle.
\tag{7}
$$

Finally, the joint state is postselected at P2, then

$$
|\Phi_f\rangle = \langle\psi_f \mid \Phi_i'\rangle
$$

$$
= \frac{1}{\sqrt{P}}\int d\omega \frac{1}{2}f(\omega)\Big[e^{i\omega\tau}\big(\cos\varepsilon - e^{i\frac{\pi\omega}{2\omega_0}}\sin\varepsilon\big)
$$

$$
- e^{-i\omega\tau}\big(\cos\varepsilon + e^{i\frac{\pi\omega}{2\omega_0}}\sin\varepsilon\big)\Big]|\omega\rangle,
\tag{8}
$$

where P is the probability of successful postselection, and

$$
P = \frac{1}{2} - \frac{1}{4}e^{-\frac{\sigma^2(\pi+4\tau\omega_0)^2}{8\omega_0^2}}\Big(1 + e^{\frac{2\pi\sigma^2\tau}{\omega_0}}\Big)\sin(2\tau\omega_0)\sin2\varepsilon
$$

$$
- \frac{1}{2}e^{-2\sigma^2\tau^2}\cos2\varepsilon\cos2\tau\omega_0.
\tag{9}
$$

According to Eq. (8), the probability distribution of the spectrum after postselection is (without normalization)

$$
F(\omega) = \big|f(\omega)\big[e^{i\omega\tau}\big(\cos\varepsilon - e^{i\frac{\pi\omega}{2\omega_0}}\sin\varepsilon\big)
$$

$$
- e^{-i\omega\tau}\big(\cos\varepsilon + e^{i\frac{\pi\omega}{2\omega_0}}\sin\varepsilon\big)\big]\big|^2.
\tag{10}
$$

The frequency shift can be calculated according to the formula $\Delta\omega = \frac{\int \omega F(\omega)d\omega}{\int F(\omega)d\omega} - \omega_0$. Thus we can obtain

$$
\Delta\omega = \frac{\sigma^2\cos(2\tau\omega_0)}{8R\omega_0 P}\big\{8T\tau\omega_0\tan(2\tau\omega_0)\cos2\varepsilon
$$

$$
+ \big[e^{\frac{2\pi\sigma^2\tau}{\omega_0}}(\pi - 4\tau\omega_0) - 4\tau\omega_0 - \pi\big]\sin2\varepsilon\big\},
\tag{11}
$$

where $R = \exp[\sigma^2(\pi + 4\tau\omega_0)^2/8\omega_0^2]$, and $T = \exp[\pi\sigma^2(\pi + 8\tau\omega_0)/8\omega_0^2]$. The corresponding wavelength shift can be obtained by the relation of $\Delta\lambda = -\frac{\lambda_0^2}{2\pi c}\Delta\omega$. In fact, the wavelength shift in this case is a rearrangement of spectral amplitudes, and

$$
\Delta\lambda = \frac{-\lambda_0\sigma^2\cos(2\tau\omega_0)}{16\pi cR\omega_0 P}\big\{8T\tau\omega_0\tan(2\tau\omega_0)\cos2\varepsilon
$$

$$
+ \big[e^{\frac{2\pi\sigma^2\tau}{\omega_0}}(\pi - 4\tau\omega_0) - 4\tau\omega_0 - \pi\big]\sin2\varepsilon\big\}.
\tag{12}
$$

Figures 2(a) and 2(b) show the variation of the output spectrum with time delay in the Im-WV scheme. It can be seen that the spectrum changes to a two-peak spectrum structure at a specific position, and the shape of the spectrum changes significantly with the increase of time delay. Therefore we can obtain the information of time delay from the new spectrum.
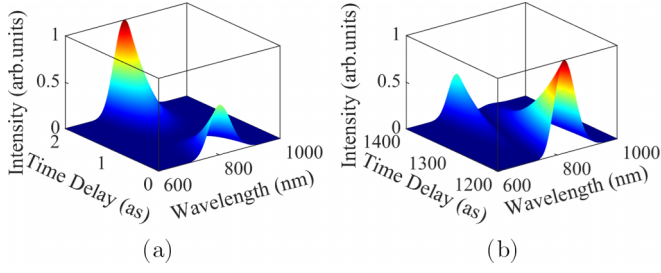
(a)   (b)

FIG. 2. The output spectrum changing with time delay in the Im-WV scheme. Here the spectral width is set to 50 nm, and the preselection angle ε is set to 0.002.

III. THE WEAK MEASUREMENT WITH REAL WEAK VALUE

Now we consider removing the QWP in Fig. 1, and the optical axes of P1 and P2 are still $\pi/4 + \varepsilon$ and $-\pi/4$, respectively. Then the preselection state and the postselection state can be represented as

$$|\psi_i\rangle_{\mathrm{Re}} = \cos(\pi/4 + \varepsilon)|H\rangle + \sin(\pi/4 + \varepsilon)|V\rangle), \quad (13)$$

$$|\psi_f\rangle_{\mathrm{Re}} = \frac{1}{\sqrt{2}}(|H\rangle - |V\rangle). \quad (14)$$

Different from the Im-WV scheme, the QWP is not used in the step of preselection, so the preselection state and postselection state are both wavelength-independent linear polarization states. In this case the weak value is purely real and a function of ε, and

$$A_{w,\mathrm{Re}} = -\cot\varepsilon. \quad (15)$$

Then the joint state with the Gaussian spectral distribution can be written as

$$|\Phi_i\rangle_{\mathrm{Re}} = \int d\omega f(\omega)[\cos(\pi/4 + \varepsilon)|H\rangle + \sin(\pi/4 + \varepsilon)|V\rangle]|\omega\rangle. \quad (16)$$

After the weak interaction, there is a time delay 2τ between $|H\rangle$ and $|V\rangle$, and the linearly polarized light becomes a group of wavelength-dependent elliptically polarized light. Then the joint state after the weak interaction can be expressed as
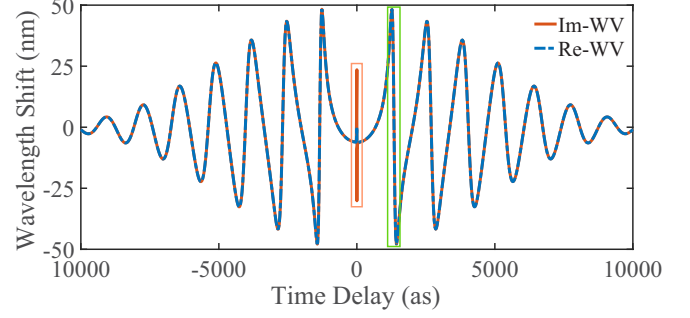
$$|\Phi_i'\rangle_{\mathrm{Re}} = \int d\omega f(\omega)[\cos(\pi/4 + \varepsilon)e^{i\omega\tau}|H\rangle + \sin(\pi/4 + \varepsilon)e^{-i\omega\tau}|V\rangle]|\omega\rangle. \quad (17)$$
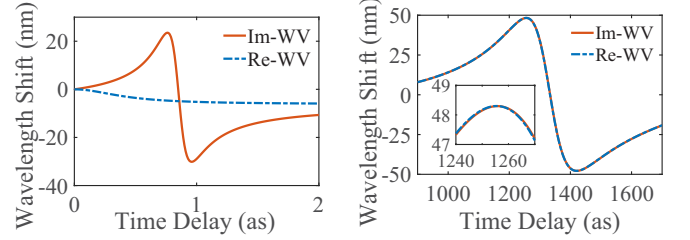
After the postselection, the pointer state collapses to

$$\begin{aligned}|\Phi_f\rangle_{\mathrm{Re}} &= \langle\psi_f|\Phi_i'\rangle_{\mathrm{Re}} \\ &= \frac{1}{\sqrt{P_{\mathrm{Re}}}} \int d\omega \frac{1}{\sqrt{2}} f(\omega)(\cos(\pi/4 + \varepsilon)e^{i\omega\tau} \\ &\quad - \sin(\pi/4 + \varepsilon)e^{-i\omega\tau})|\omega\rangle,\end{aligned} \quad (18)$$

where P_{Re} is the probability of successful postselection,

$$P_{\mathrm{Re}} = \frac{1}{2}\left(1 - e^{-2\sigma^2\tau^2}\cos 2\varepsilon \cos 2\tau\omega_0\right). \quad (19)$$

(a)

(b)   (c)

FIG. 3. (a) Periodic changes of the wavelength shift $\Delta\lambda$ with time delay τ in the Re-WV scheme and Im-WV scheme. The orange box marks zone 0, and the green box marks zone 1. (b) and (c) are the $\Delta\lambda$ in zone 0 and zone 1, respectively. Here the spectral width is set to 50 nm, and the preselection angle ε is set to 0.002.

The probability distribution of frequency is (without normalization)

$$F(\omega)_{\mathrm{Re}} = |f(\omega)|^2(1 - \cos 2\varepsilon \cos 2\tau\omega). \quad (20)$$

The change of spectrum leads to the shift of frequency pointer

$$\Delta\omega_{\mathrm{Re}} = \frac{2\sigma^2\tau \cos 2\varepsilon \sin 2\tau\omega_0}{e^{2\sigma^2\tau^2} - \cos 2\varepsilon \cos 2\tau\omega_0}, \quad (21)$$

and then the corresponding wavelength shift is

$$\Delta\lambda_{\mathrm{Re}} = \frac{-\lambda_0\sigma^2\tau \cos 2\varepsilon \sin(2\tau\omega_0)}{\pi c\left(e^{2\sigma^2\tau^2} - \cos 2\varepsilon \cos 2\tau\omega_0\right)}. \quad (22)$$

In order to show the difference between the Im-WV scheme and the Re-WV scheme in high-precision parameter measurement, we explore them in detail. Figure 3 shows the wavelength shift with respect to the time delay τ. Here the light source with central wavelength of 800 nm and spectral width of 50 nm is chosen, and the preselection angle ε is set to 0.002. As shown in Fig. 3(a), with the change of time delay, the wavelength shift changes sharply in some regions, which means that the parameter measurement in these regions will have high sensitivity, so we define these regions as the working region. The orange and green boxes mark zone 0 and zone 1, respectively. Figures 3(b) and 3(c) show the variation trend of wavelength shift with time delay in zone 0 and zone 1. It can be seen that the wavelength shift of the Re-WV scheme is smaller than that of the Im-WV scheme in zone 0, while the two schemes are similar in zone 1. Since the preselection state of the Im-WV scheme has an initial phase, the two curves in Fig. 3(c) do not overlap completely, but the overall trends
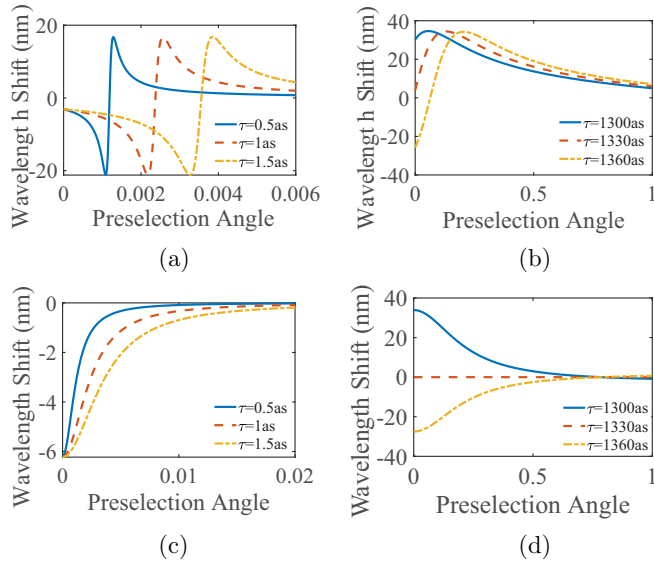
(a)

(b)

(c)

(d)

FIG. 4. The wavelength shift $\Delta\lambda$ with respect to the preselection angle ε and time delay τ in the Re-WV scheme and the Im-WV scheme. (a) and (b) are the $\Delta\lambda$ of zone 0 and zone 1 in the Im-WV scheme, respectively. (c) and (d) are the $\Delta\lambda$ of zone 0 and zone 1 in the Re-WV scheme, respectively. Here the spectral width is set to 50 nm.

(a)

(b)

(c)

FIG. 5. (a) The wavelength shift rate with respect to the time delay τ in the Re-WV scheme and the Im-WV scheme. (b) The postselection probability with respect to the time delay τ in the Re-WV scheme and the Im-WV scheme. Here the spectral width is set to 50 nm, and the preselection angle ε is set to 0.002. (c) The maximum wavelength shift rate with respect to the spectral width in the Re-WV scheme and the Im-WV scheme.

of the two are still consistent. This means that there is a significant difference in measurement precision between the two schemes only in zone 0.

Figure 4 shows the relationship between wavelength shift and preselection angle in Im-WV and Re-WV schemes. As shown in Figs. 4(a) and 4(b), the preselection angle is the initial phase of the preselection state and its change will cause adjustment to the working region in the Im-WV scheme. Figures 4(c) and 4(d) show that adjusting the preselection angle in the Re-WV scheme only affects the wavelength shift rate rather than the working region. However, the introduction of a phase compensator allows for the experimental adjustment of the working region. In the Re-WV scheme, the wavelength in zone 0 is only shift to the short-wavelength direction, and the direction of wavelength shift in zone 1 is only related to the time delay. It can be seen that the wavelength shift rate of both the two schemes decreases with the increase of the preselection angle.

In order to compare the difference between the two schemes in zone 0, we use the wavelength shift rate $d\Delta\lambda/d\tau$ to characterize the measurement sensitivity. The wavelength shift rate [Fig. 5(a)] and postselection probability [Fig. 5(b)] of the Im-WV scheme and the Re-WV scheme were compared. The green boxes in the figures mark the regions with the highest wavelength shift rate of the two schemes. Compared with the Im-WV scheme, the wavelength shift rate of Re-WV scheme is two orders of magnitude lower, but the postselection probability is two orders of magnitude higher. The higher the postselection probability, the easier it is to be observed experimentally. Figure 5(c) shows the relationship between the maximum wavelength shift rate of the two schemes and the spectral width in zone 0. With the increase of the spectral width, the wavelength shift rate of Im-WV scheme increases
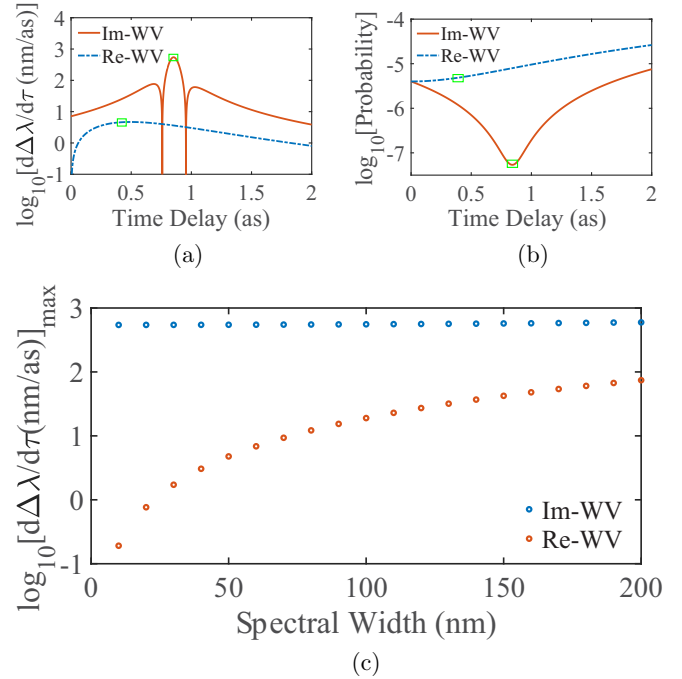
slightly, while that of Re-WV scheme increases significantly. It can be seen that with the increase of spectral width, the sensitivity difference between the two schemes gradually decreases.

Now we discuss the effect of time delay on the spectrum in the Re-WV scheme, which will allow us to further understand the reason for the wavelength shift in the Re-WV scheme. As shown in Fig. 6(a), after the weak interaction, a phase difference of $2\omega\tau$ is generated between the horizontal and vertical polarization components in zone 0, and the linearly polarized light becomes a group of wavelength-dependent elliptically polarized light. The shorter the wavelength, the farther from the orthogonality between the preselection state and the postselection state, and the higher the probability of passing through the polarizer P2 in the step of postselection. From Figs. 6(c) and 6(d), it can be seen that as the time delay increases, the center of the Gaussian wave packet gradually shifts to the short-wavelength direction. At the same time, the amplitude of the spectrum is also increasing because the postselection probability is a function of the time delay τ.

In zone 1, as shown in Fig. 6(b), the linearly polarized light becomes a group of elliptically polarized light with a phase difference of about 2π after the interaction. When the phase difference produced by a certain wavelength is exactly 2π, the light of this wavelength evolves into linearly polarized light with the same polarization direction as the preselection state, and then the postselection probability of this wavelength will be minimum. So other wavelengths have a relatively
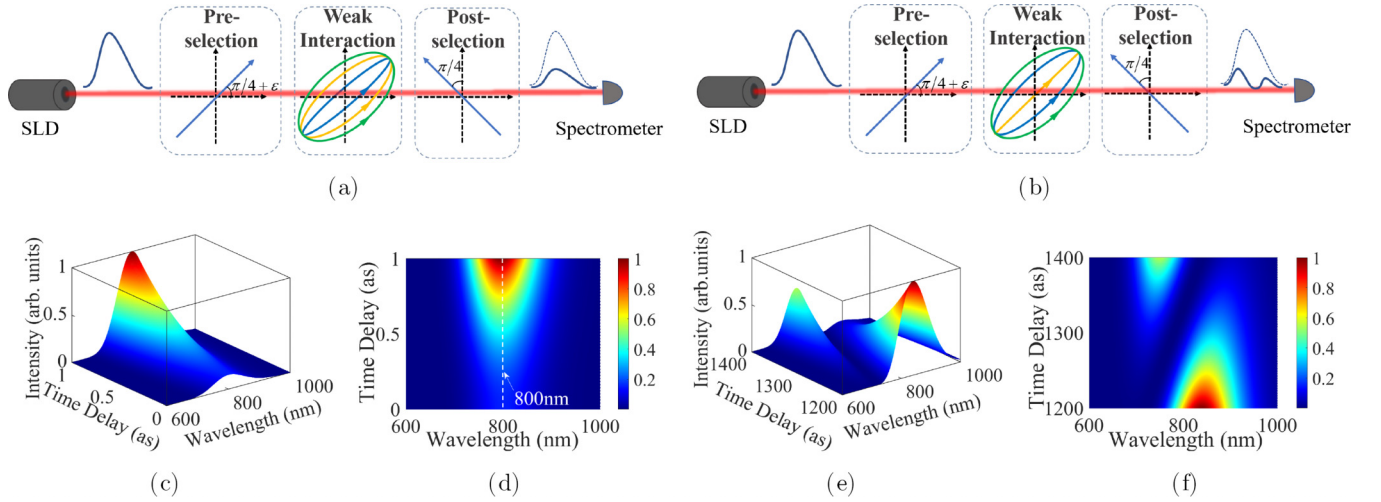
FIG. 6. (a) The polarization components in zone 0 of the three steps in the Re-WV weak measurement scheme. (b) The polarization components in zone 1 of the three steps in the Re-WV weak measurement scheme. (c) and (d) are the output spectrum changing with time delay and its top view in zone 0, respectively. The black dotted line in (c) indicates that the central wavelength of the input Gaussian spectrum is 800 nm. (e) and (f) are the output spectrum changing with time delay and its top view in zone 1, respectively. Here the spectral width is set to 50 nm and the preselection angle ε is set to 0.002.

higher probability of passing through the polarizer P2, and the Gaussian wave packet has a valley bottom and splits into two wave packets. As shown in Figs. 6(e) and 6(f), with the time delay increases, the position of the valley bottom moves to the long-wavelength direction. The Gaussian wave packet is split from one to two, and then returns to one. Figure 7 shows the output spectrum distribution of the Re-WV scheme for different time delays at the positions of the highest precision in zone 0 [Fig. 7(a)] and zone 1 [Fig. 7(b)]. In zone 0, with the increase of time delay, the peak of the spectrum increases and gradually shifts to the short-wavelength direction. In zone 1 the output spectrum distribution in the working region presents a two-peak spectrum structure, and the change of time delay can lead to a significant change of the spectrum. However, the working region of zone 1 corresponds to a large range of time delay, so its measurement sensitivity is not as high as that of zone 0. In the experiment we can use a Soleil-Babinet compensator or a pair of half-wave plates to compensate the phase delay to the sensitive region to maximize the measurement precision [14,22].
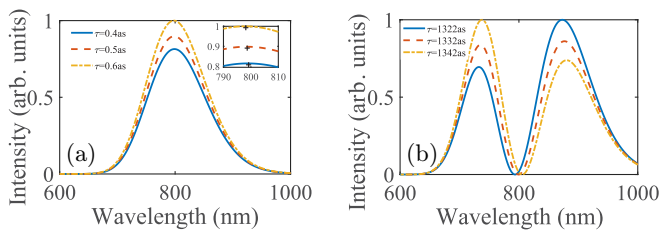

FIG. 7. (a) The output spectrum distribution of the Re-WV scheme for different time delays in zone 0. The sign "+" indicates the position of the peak of these wave packets. (b) The output spectrum distribution of the Re-WV scheme for different time delays in zone 1. Here the spectral width is set to 50 nm, and the preselection angle ε is set to 0.002.

The estimation precision limit for parameter is given by Cramér Rao bound (C-R bound) [23,24]

$$\delta\tau \geqslant \frac{1}{\sqrt{NI_\tau}}. \tag{23}$$

In this scheme, N is the number of photons and I_τ is the Fisher information. For a given quantum state, we can try different measurement schemes to maximize the Fisher information that can be obtained. The maximum Fisher information is called quantum Fisher information (QFI), which is the upper bound of the Fisher information, and the precision limit corresponds to the quantum C-R bound. In the Re-WV scheme, the QFI [10]

$$Q = 4\left[\left(\frac{\partial\langle\Phi_i'|_{\text{Re}}}{\partial\tau}\right)\left(\frac{\partial|\Phi_i'\rangle_{\text{Re}}}{\partial\tau}\right) - \left|\langle\Phi_i'|_{\text{Re}}\left(\frac{\partial|\Phi_i'\rangle_{\text{Re}}}{\partial\tau}\right)\right|^2\right]$$
$$= 4[\langle\omega^2\rangle_0 - \sin^2 2\varepsilon(\omega_0)^2], \tag{24}$$

where the QFI is based on the quantum state $|\Phi_i'\rangle_{\text{Re}}$. This indicates that QFI is only related to the measurement pointer and the preselection state of the system. In the weak measurement scheme, we only focus on the part of the information that is successfully postselected. The Fisher information is [25,26]

$$I_\tau = P_{\text{Re}} \int \frac{1}{F(\omega)_{\text{Re}}}\left(\frac{\partial F(\omega)_{\text{Re}}}{\partial\tau}\right)^2 d\omega, \tag{25}$$

where $F(\omega)_{\text{Re}}$ is the normalized probability distribution of frequency in the Re-WV scheme and

$$F(\omega)_{\text{Re}} = |f(\omega)|^2 \frac{1 - \cos 2\varepsilon \cos 2\tau\omega}{1 - e^{-2\sigma^2\tau^2}\cos 2\varepsilon \cos 2\tau\omega_0}. \tag{26}$$

Since the time delay is difficult to measure directly, we usually obtain the time delay to be measured indirectly through an observable ω. In the experiment we estimate the time delay τ by observing the frequency shift of the spectrum, so we can estimate the error due to fluctuation in the process of
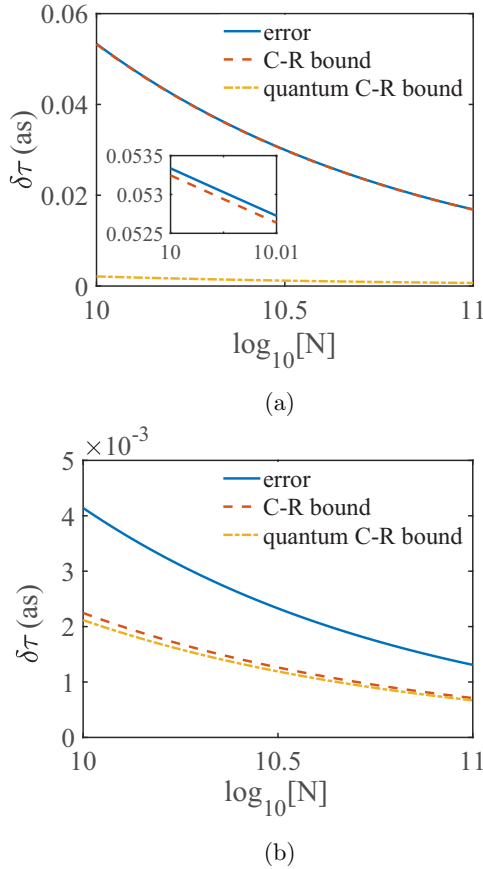
(a)

(b)

FIG. 8. (a) The measurement precision limit $\delta\tau$ with respect to the number of photons N in zone 0. (b) The measurement precision limit $\delta\tau$ with respect to the number of photons N in zone 1. Here the time delay takes the value $\tau = 1$ as and $\tau = 1350$ as, respectively. The spectral width is set to 50 nm, and the preselection angle ε is set to 0.002.

measurement from the error propagation formula [27]

$$\delta\tau_{err} = \frac{\sqrt{\langle (\Delta\omega)^2_{\mathrm{Re}} \rangle - \langle \Delta\omega \rangle^2_{\mathrm{Re}}}}{\sqrt{NP_{\mathrm{Re}}} |\partial \langle \Delta\omega \rangle_{\mathrm{Re}} / \partial\tau|}. \tag{27}$$

The quantum C-R bound represents the optimal precision limit that can be obtained on the joint quantum state $|\Phi'_i\rangle_{\mathrm{Re}}$, and the C-R bound represents the precision limit that can be obtained in the measurement scheme. As shown in Fig. 8, while the precision limit in zone 0 deviates significantly from the quantum C-R bound, the precision limit of zone 1 is very close to it. Although it is more sensitive than zone 1, the Fisher information of zone 0 is much smaller than the QFI due to the small probability of successful postselection, so the precision limit of zone 0 is worse than that of zone 1. In the experiment,

the high-brightness light source is usually selected to compensate for the information loss caused by the postselection. This result means that the Re-WV scheme can also be used for precision measurement in the frequency domain. This is different from the conclusion that only imaginary weak value can be used for parameter estimation in previous studies. Therefore in some parameter measurement experiments, we do not need to focus on constructing the imaginary weak value, since the experimental setup and data processing of the Re-WV scheme is more straightforward.

IV. CONCLUSION

In this paper we have discussed a weak measurement scheme with real weak value in the frequency domain. We have performed a detailed derivation of this scheme and compared it with the Im-WV scheme. The purely real weak value can also cause the wavelength shift related to the measured parameters in the broad-spectrum weak measurement. The reasons for the wavelength shift and the regularity of the spectral change are analyzed. It can be seen from the simulation results that the Re-WV scheme can obtain the same wavelength shift and measurement precision as the Im-WV scheme in the working regions except zone 0. By calculating the Fisher information and the precision limit of the Re-WV scheme, it is found that the C-R bound in zone 1 is close to the quantum C-R bound. We also calculate the fluctuation of the time delay to be measured in this measurement scheme. These results prove that the Re-WV scheme can be used to measure parameters with high precision.

We conclude that the real weak value can also be used for high-precision measurement of parameters in the frequency-domain weak measurement. At the same time, the QWP is not needed in the experimental setup of the Re-WV scheme, so the error caused by the broad-spectrum light source passing through the wave plate in the step of preselection does not need to be considered, and simplifying the optical components can also reduce the source of error. It is meaningful to reduce the source of error in precision measurement.

[1] Y. Aharonov, D. Z. Albert, and L. Vaidman, How the result of a measurement of a component of the spin of a spin-1/2 particle can turn out to be 100, Phys. Rev. Lett. **60**, 1351 (1988).

[2] P. B. Dixon, D. J. Starling, A. N. Jordan, and J. C. Howell, Ultrasensitive beam deflection measurement via interferometric weak value amplification, Phys. Rev. Lett. **102**, 173601 (2009).

[3] O. Hosten and P. Kwiat, Observation of the spin Hall effect of light via weak measurements, Science **319**, 787 (2008).

[4] D. J. Starling, P. B. Dixon, A. N. Jordan, and J. C. Howell, Optimizing the signal-to-noise ratio of a beam-deflection measurement with interferometric weak values, Phys. Rev. A **80**, 041803(R) (2009).

[5] G. I. Viza, J. Martínez-Rincón, G. A. Howland, H. Frostig, I. Shomroni, B. Dayan, and J. C. Howell, Weak-values technique for velocity measurements, Opt. Lett. **38**, 2949 (2013).

[6] R. Jozsa, Complex weak values in quantum measurement, Phys. Rev. A **76**, 044103 (2007).

[7] X. Y. Xu, Y. Kedem, K. Sun, L. Vaidman, C. F. Li, and G.-C. Guo, Phase estimation with weak measurement using a white light source, Phys. Rev. Lett. **111**, 033604 (2013).

[8] C. F. Li, X. Y. Xu, J. S. Tang, J. S. Xu, and G. C. Guo, Ultrasensitive phase estimation with white light, Phys. Rev. A **83**, 044102 (2011).

[9] Z. H. Zhang, G. Chen, X. Y. Xu, J. S. Tang, W. H. Zhang, Y. J. Han, C. F. Li, and G. C. Guo, Ultrasensitive biased weak measurement for longitudinal phase estimation, Phys. Rev. A **94**, 053843 (2016).

[10] F. Li, J. Z. Huang, and G. H. Zeng, Adaptive weak-value amplification with adjustable postselection, Phys. Rev. A **96**, 032112 (2017).

[11] D. M. Li, Z. Y. Shen, Y. H. He, Y. L. Zhang, Z. L. Chen, and H. Ma, Application of quantum weak measurement for glucose concentration detection, Appl. Opt. **55**, 1697 (2016).

[12] Y. J. Zhang, L. X. Shi, Y. Xu, X. Zheng, J. W. Li, Q. Wu, S. X. Li, and Y. H. He, Optical quantum weak measurement coupled with UV spectrophotometry for sensitively and non-separately detecting enantiopurity, Opt. Express **27**, 9330 (2019).

[13] Y. Xu, L. X. Shi, S. X. Li, T. Guan, S. Y. Zhong, X. S. Zhou, D. M. Li, C. X. Guo, Y. X. Yang, X. N. Wang, Z. Y. Li, Y. H. He, L. Y. Xie, and Z. H. Gan, Detection of macromolecular content in a mixed solution of protein macromolecules and small molecules using a weak measurement linear differential system, Anal. Chem. **18**, 91 (2019).

[14] Y. S. Wang, S. Z. Chen, S. C. Wen, and H. L. Luo, Realization of ultra-small stress birefringence detection with weak-value amplification technique, Appl. Phys. Lett. **118**, 161104 (2021).

[15] Y. He, L. Luo, L. G. Xie, J. Y. Shao, Y. R. Liu, J. C. You, Y. C. Ye, and Z. Y. Zhang, Detection of magneto-optical Kerr signals via weak measurement with frequency pointer, Opt. Lett. **46**, 4140 (2021).

[16] N. Brunner and C. Simon, Measuring small longitudinal phase shifts: Weak measurements or standard interferometry? Phys. Rev. Lett. **105**, 010405 (2010).

[17] H. J. Li, Y. J. Li, J. Z. Huang, M. M. Liu, and G. H. Zeng, Ultra-sensitive measurement of third-order optical nonlinearity via weak value amplification, Appl. Phys. Lett. **114**, 161906 (2019).

[18] D. Li, C. Weng, Y. Ruan, K. Li, G. Cai, C. Song, Q. Lin, An optical chiral sensor based on weak measurement for the real-time monitoring of sucrose hydrolysis, Sensors **21**, 1003 (2021).

[19] J. R. Zhao, Z. J. Wu, G. Q. Wang, C. N. Wang, B. F. Deng, and S. Q. Sun, Optical weak measurement for the precise thickness determination of an ultra-thin film, Appl. Opt. **61**, 10065 (2022).

[20] Y. S. Wang, W. S. Zhang, S. Z. Chen, S. C. Wen, and H. L. Luo, Multiple-weak-value quantum measurement for precision estimation of time delay, Phys. Rev. A **105**, 033521 (2022).

[21] J. C. Howell, Weakness of weak values: Incompatibility of anomalous pulse-spectrum amplification and optical frequency combs, Phys. Rev. A **106**, 012224 (2022).

[22] X. D. Qiu, L. G. Xie, X. Liu, L. Luo, Z. X. Li, Z. Y. Zhang, and J. L. Du, Precision phase estimation based on weak-value amplification, Appl. Phys. Lett. **110**, 071105 (2017).

[23] S. L. Braunstein and C. M. Caves, Statistical distance and the geometry of quantum states, Phys. Rev. Lett. **72**, 3439 (1994).

[24] J. Martínez-Rincón, W. T. Liu, G. I. Viza, and J. C. Howell, Can anomalous amplification be attained without postselection? Phys. Rev. Lett. **116**, 100803 (2016).

[25] L. J. Zhang, A. Datta, and I. A. Walmsley, Precision metrology using weak measurements, Phys. Rev. Lett. **114**, 210801 (2015).

[26] R. A. Fisher, in *Statistical Science* (Institute of Mathematical Statistics, Waite Hill, OH, 1997), Vol. 12, pp. 39–41.

[27] X. Guo, C. R. Breum, J. Borregaard, S. Izumi, M. V. Larsen, T. Gehring, M. Christandl, J. S. Nielsen, and U. L. Andersen, Distributed quantum sensing in a continuous-variable entangled network, Nat. Phys. **16**, 281 (2020).